Water activation measurements in JET basement during DD and DT operations

Plasma Physics and Controlled Fusion

OPEN ACCESS

RECEIVED
22 October 2025

REVISED
25 February 2026

ACCEPTED FOR PUBLICATION
13 March 2026

PUBLISHED
24 March 2026

PAPER

Water activation measurements in JET basement during DD and DT operations

Julijan Peric[1,*], Domen Govekar[1], Sebastjan Rupnik[1], Luka Snoj[1], Rosaria Villari[2], Nicola Fonnesu[2], Stefano Loreti[2], Perry Beaumont[3], Slawomir Mianowski[3], Callum Grove[3], Luke Jones[3], Tom Berry[3], Chantal Shand[3], Anthony Turner[3], Haridev Chohan[3], Paul Carman[3], Robert Lobel[3], Marco De Pietri[4], Eduardo Masia[5], Aljaž Kolšek[5], Raul Pampin[5], Pierluigi Chiovaro[6], Vladimir Radulović[1] and JET contributors[7]

[1] Jožef Stefan Institute, Jamova cesta 39, SI-1000 Ljubljana, Slovenia
[2] ENEA Frascati, Via Enrico Fermi, 45, Frascati, RM 00044, Italy
[3] UKAEA, Culham Campus, Abingdon, Oxfordshire OX14 3DB, United Kingdom
[4] Departamento de Ingeniería energética, UNED, Calle Juan del Rosal 12, Madrid 28040, Spain
[5] Fusion for Energy, Josep Pla 2 B3, Barcelona 08019, Spain
[6] Department of Engineering, University of Palermo, Viale delle Scienze, Ed. 6, 90128 Palermo, Italy
[7] See Maggi *et al* 2024 (https://doi.org/10.1088/1741-4326/ad3e16) for JET contributors.
[*] Author to whom any correspondence should be addressed.

E-mail: julijan.peric@ijs.si

Keywords: water activation experiment, JET, safety, fluid activation, MCNP

Abstract

In water-cooled D–T fusion tokamaks such as the Joint European Torus (JET), neutron activation of flowing water produces short-lived radionuclides that generate a distributed high-energy gamma and neutron radiation source in the water cooling circuit. The energy and intensity of the source are crucial factors in the design of cooling and shielding systems in future water-cooled deuterium–tritium fusion tokamaks such as ITER. While several past experiments provide fusion-relevant experimental data on water activation, the JET water activation experiment carried out during the 2023 DD and DT campaigns is the first such experiment in a fusion tokamak environment. In the water activation experiment at JET, two types of scintillation detectors were used to measure gamma rays from activated water in the basement below JET Octant 4. The system successfully recorded and processed data from over 1500 JET pulses, including both DD and DT operations, providing a robust data set for analyzing N-16 activity in cooling water. This manuscript describes the preparation of the JET water activation experiment, the calibration of the detectors and the analysis of the experimental data.

1. Introduction

The Joint European Torus (JET), the largest operational fusion research facility until the end of its scientific operation in December 2023, provided a unique opportunity to conduct water activation experiments in a representative fusion environment. A water activation experiment at JET (WACT) was proposed in 2017 to support the design and safety assessment of ITER, a water-cooled deuterium–tritium (DT) fusion reactor currently under construction in Cadarache, France. The aim was to measure the neutron-induced activation of water and determine the resulting activity levels, with a focus on N-16 production [1, 2].

Water activation occurs through neutron-induced nuclear reactions on the oxygen isotopes present in cooling water, producing short-lived radioactive nuclei. In fusion environments, fast neutrons interact mainly with O-16, O-17, and O-18, generating activation products such as N-16, N-17, and O-19. These radionuclides decay within a few to several tens of seconds, emitting high-energy gamma rays and, in the case of N-17, delayed neutrons. Activated water therefore constitutes a time-dependent radiation source, with intensity directly determined by the neutron flux and energy distribution.

The neutron energy spectrum differs substantially between deuterium–deuterium (DD) and DT fusion plasmas, having a decisive impact on water activation. DD fusion produces neutrons with energies around 2.45 MeV, which are below the threshold for most oxygen activation reactions and therefore result in limited activation. In contrast, DT fusion generates 14.1 MeV neutrons, enabling threshold reactions such as $^{16}O(n,p)^{16}N$ and $^{17}O(n,p)^{17}N$, leading to significantly increased activation levels [3, 4].

Initial feasibility studies, including Monte Carlo simulations to estimate the expected activity values, the identification of the detectors and their experimental calibration, were carried out between 2017 and 2018. The proposed experiment could not be performed during the JET DT Experiment-2 in 2021 due to resource constraints. In preparation for the JET DT Experiment-3 (DTE3), the design of the water activation experiment was finalized in collaboration with the "Jožef Stefan" Institute, the Italian National Agency for New Technologies, Energy and Sustainable Economic Development (ENEA) and The UK Atomic Energy Authority (UKAEA) as part of the EUROfusion work package Preparation of ITER Operation (WPPrIO). The WACT experiment was successfully conducted during the 2023 DD and DT campaigns at JET. The results are presented in this paper [5–7].

2. Water activation experiment at JET

Two JET cooling circuits were initially considered for the water activation experiment: the divertor cooling pipes and the neutral beam injector (NBI) duct scraper cooling pipes [8]. The selection was based on three main criteria: (i) the water had to be exposed to D–T fusion neutrons with energies greater than 10 MeV; (ii) the transit time of the activated water from the region inside the vessel to the detector location had to be comparable to the half-life of N-16; and (iii) it had to be possible to position the detector(s) in close proximity to the tube.

Based on these considerations, the NBI duct scraper cooling pipes were selected [1]. Two potential locations for the installation of the water activation experiment were identified in the basement of the JET tokamak: beneath Octant 4 and Octant 8. Octant 8 was initially selected due to the available space around the vertical cooling pipe. However, during the design phase, technical limitations related to the construction and mechanical support of the experiment made this option impractical. Consequently, before the DTE3 campaign, the installation site was relocated to the area beneath Octant 4, where the experiment was positioned under the horizontal cooling pipe. After this relocation, it was found that the radiation shielding previously designed was incompatible with the new installation geometry. As a result, a new shielding assembly was designed and constructed. The final configuration of the experiment is presented in figure 1.

3. Experimental setup

The experimental setup was divided into two parts: the data acquisition system (DAQ) in the WACT cubicle (KM8) in the JET cubicle building presented in figure 2 and the detector system in the JET basement under Octant 4 [7, 9].

The high voltage for both detectors was provided by two ORTEC 556 high-voltage power supplies. The NaI detector was operated at −650 V, while the bismuth germanat (BGO) detector was biased at +1400 V. The signals were digitized using a CAEN DT5730S digitizer (8 channels, 14 bit resolution, 500 MS s^{-1} sampling rate) in combination with data acquisition software Phoenix developed by ENEA. The system was connected to the JET CODAS infrastructure. Data acquisition was automatically triggered by the JET pulse start signal and lasted 300 s [10].

The detector system consisted of a BGO detector and a sodium iodide (NaI) detector, mounted on separate detector tables, each fitted with a 3" × 3" (7.62 cm × 7.62 cm) scintillation crystal. Both detectors were located directly under the NBI duct scraper water cooling pipe. To reduce background radiation, each detector was located in a lead shielding enclosure constructed from chevron blocks (≈25 cm × 25 cm × 20 cm).

Lead collimator plates, i.e. square 1.3 cm thick lead plates with a central circular aperture either 5 mm in diameter (small collimator) or 30 mm in diameter (medium collimator), were placed above the detectors to define the detection geometry and increase the measurement sensitivity to the activated water volume in the immediate vicinity of the detectors, as opposed to the whole extent of the cooling pipe. The experimental setup presented is shown in figure 3. Different collimators were used in different phases of the experiment, which are shown in table 1.

The collimator configurations used during the various experimental phases were selected based on Monte Carlo N-particle code (MCNP) simulations and the expected activation levels of the cooling water under the corresponding JET operating conditions. During DD operation, water activation is

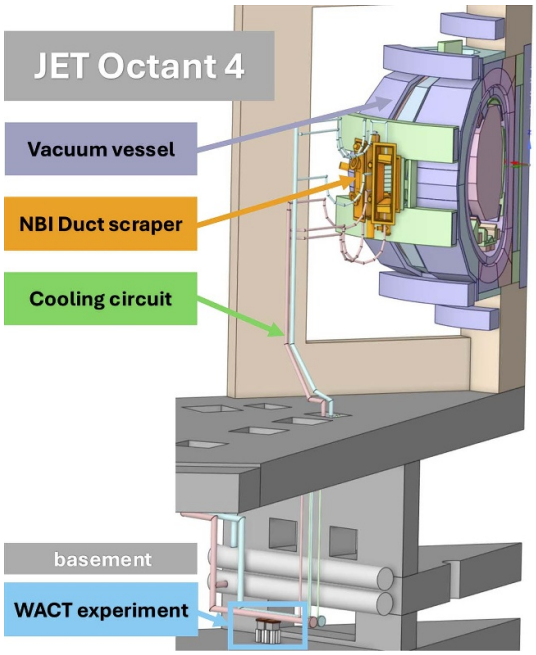

Figure 1. JET Octant 4 model with NBI duct scraper, NBI duct scraper cooling pipes and WACT experiment located in the basement.

Figure 2. Setup of the WACT cubicle during the test with a ^{60}Co calibration source. The gamma spectra were recorded with two different data acquisition software systems for comparative analysis.

mainly driven by residual tritium, as DD neutrons have energies below the threshold of the O-16(n,p)N-16 reaction, resulting in low expected activity and count rates. In this case, non-collimated or weakly collimated configurations were used to maximize detection efficiency. The DD campaign provided operational experience with detector response and count rates, forming the basis for extrapolating expectations and selecting suitable collimator configurations for the DTE3 campaign. In contrast to DD operation, during DT operation, the 14.1 MeV neutrons are above the reaction threshold, leading to significantly higher expected activation levels. Tighter collimation was therefore employed to control count rates and enhance sensitivity to the activated water volume near the detectors [11].

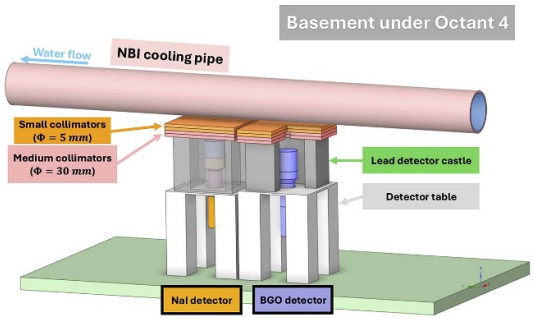

Figure 3. The WACT detector system located in the basement below JET Octant 4. The collimator plate configuration matches the one in place for the DTE3 campaign at JET.

Table 1. Collimator configurations for NaI and BGO detectors used in the WACT experiment at JET from June 2023 to January 2024, listed by operating period and campaign.

Time period	Campaign	NaI	BGO
9 June–9 August 23	DD—C45	Ø	Ø
9–17 August 23	DD—C45	2 × medium	2 × medium
17–27 August 23	DD—C45	Ø	2 × small
27 August–26 September 23	DTE3—C46	2 × medium + 2 × small	2 × medium + 2 × small
26 September–22 November 23	C46 + C47	4 × no hole	2 × medium + 2 × small
22–28 November 23	DD—C47	Ø	Ø
15–18 January 24	Calibration	Ø	Ø

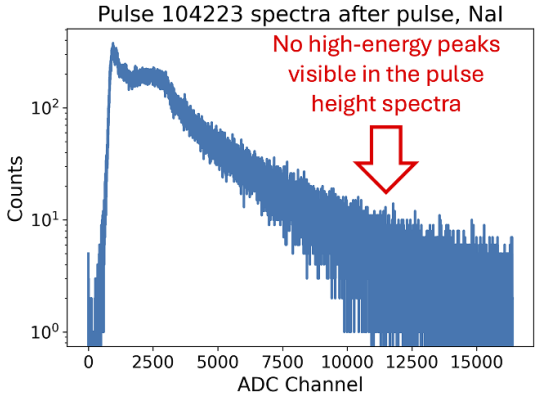

Figure 4. NaI pulse height spectrum after JET pulse no. 104 223. No high-energy peaks are visible in the pulse height spectrum due to N-16 (9 August 2023).

3.1. Detector limitations and exclusion criteria

During the three JET experimental campaigns (C45–DD, C46–DTE3, C47–Clean-up DD) from August to December 2023, over 1500 JET pulses were recorded with the experimental setup presented. Several issues were noticed with the data recorded from the NaI detector, notably pulse pile-up and energy drifting, which prevented the reliable identification of the N-16 peaks. It is worth noting that the NaI detector was optimized for low count rate applications. Figure 4 displays a typical γ pulse height spectrum obtained with the NaI detector (pulse 104 223).

Therefore, in the following sections, only results obtained with the BGO detector that meet the physical relevance and data quality criteria are presented. The analysis focuses on DT-relevant conditions; DD data, dominated by residual tritium and sub-threshold neutron energies, were therefore excluded. For the DTE3 campaign, additional exclusion criteria were applied based on detector performance and system stability, as a significant fraction of pulses exhibited detector saturation or data acquisition system transfer limitations, resulting in overexposed spectra that could not be reliably analyzed with the methodology presented.

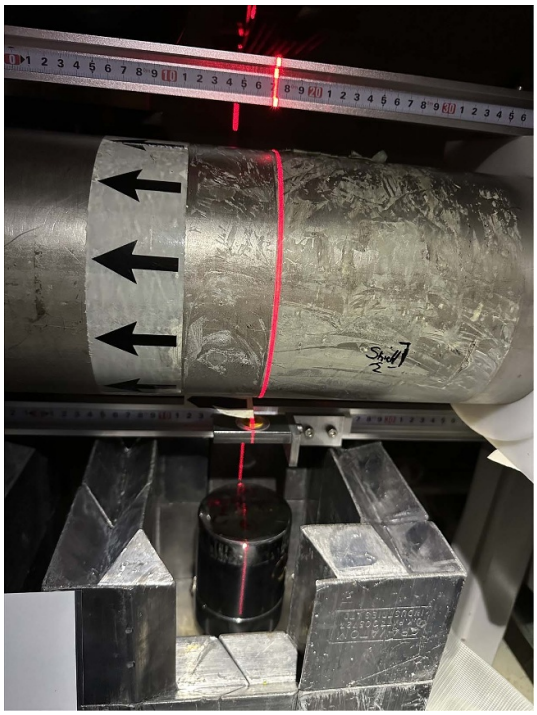

Figure 5. BGO detector setup during efficiency calibration. The source is located in the center above the detector under the water cooling pipe. A vertical laser line was used to accurately position the calibration sources.

4. Detector calibration

The determination of the N-16 activity by gamma spectrometry requires detection efficiency data at high energies: 6.128 MeV and 7.115 MeV. Experimental detection efficiency curves are usually generated on the basis of measured efficiencies using calibration sources up to around 3 MeV and fitting with 4th to 6th order polynomials [12]. Since there are no calibration sources available with energies above this range, direct experimental calibration at N-16 energies is not possible [13].

A combined experimental–computational approach was used to estimate the detection efficiency of the experimental system presented in figure 5. Calibration measurements were performed at lower energies ($E < 1.5$ MeV) and the corresponding efficiencies were determined. The MCNP code was used to calculate an efficiency curve for a point source geometry corresponding to the calibration setup and scaled to match the measured data.

The first test measurement with calibration sources was carried out in June 2023. As the experimental setup had not yet been completed, the data obtained during the first test calibration was only used to check the functionality of the system. The second calibration measurement took place in June 2024 after the last scientific JET campaign with the final WACT experimental setup.

4.1. Energy calibration

The energy calibration of the gamma spectrometry system was performed with the summed signal spectra of the first four JET DTE3 pulses (104 128–104 131). The calibration spectra recorded with the BGO detector and the corresponding gamma peaks are shown in figure 6. A linear function was used to relate the ADC channel numbers to the gamma ray energies, defined as

$$E = k \cdot X + C_0,$$

with $k = 9.8 \cdot 10^{-3} \pm 3.0 \cdot 10^{-5}$ MeV/channel and $C_0 = 5.1 \cdot 10^{-2} \pm 1.4 \cdot 10^{-2}$ MeV. This calibration curve was derived from the identified peak positions of Cs-137 (0.662 MeV), Co-60 (1.173 MeV and 1.333 MeV) and N-16 (5.577 MeV, 6.129 MeV and 7.115 MeV). The first three peaks originate from a multi-gamma source (AL-2735) installed in the lead shielding of the detector and present throughout the measurements, the last three from activated water itself.

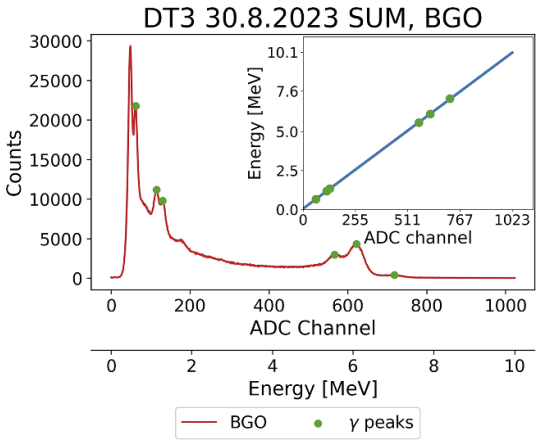

Figure 6. Summed gamma spectra recorded with the BGO detector during the first four DTE3-JET pulses. The pulse height spectrum was re-binned with a factor of 64. Distinctive gamma-ray peaks used for energy calibration are marked. The inset shows a linear fit of the energy–channel relationship based on the identified peaks (30 August 2023).

Table 2. Experimental and calculated BGO detection efficiencies.

Radionuclide	Energy [MeV]	Measured	Calculated	Corrected
Cs-137	0.661	0.0258 (±3.0%)	0.0268 (±0.30%)	0.0267 (±0.31%)
Co-60	1.173	0.0209 (±3.1%)	0.0206 (±0.30%)	0.0205 (±0.31%)
Co-60	1.332	0.0189 (±3.0%)	0.0192 (±0.30%)	0.0192 (±0.31%)
N-16	6.128	N/A	0.0096 (±0.25%)	0.00 953 (±0.26%)
N-16	7.115	N/A	0.0090 (±0.26%)	0.00 893 (±0.27%)

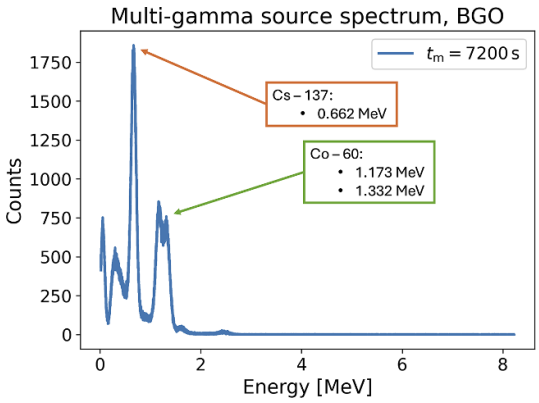

Figure 7. Calibration spectra acquired with the BGO detector using multi gamma source (AL-2735). The annotated gamma peaks were used to correct the calculated BGO detector efficiency. The measurement duration was $t_m = 7200$ s (15 June 2024).

4.2. Efficiency calibration

Computational models of the NaI and BGO detectors were developed using MCNP, based on the available manufacturer data. Calculations of pulse height spectra were performed by means of the pulse-height estimator (F8 tally in MCNP terminology). Additionally, to obtain realistic pulse height spectra from the calculations, the option of Gaussian energy broadening (GEB) was used. The GEB parameters were determined on the basis of past measurements with the same detectors [1].

Detection efficiency curves were calculated by means of an isotropic point photon source with equiprobably energy (1000 energy bins in total from 0 to 10 MeV, $\Delta E = 10$ keV) and the F8 pulse height tally. The SCX option was used, which subdivides the calculated result, i.e. the pulse height spectrum on the basis of the sampled index of a specified source distribution, in this case the gamma energy distribution. The reference source-to-detector distance was 88 mm. The calculated efficiency curve was scaled using a least-squares fit to best match the experimental values, resulting in an optimal scaling factor of 0.9997. The measured calibration spectra using multi gamma source is presented in figure 7.

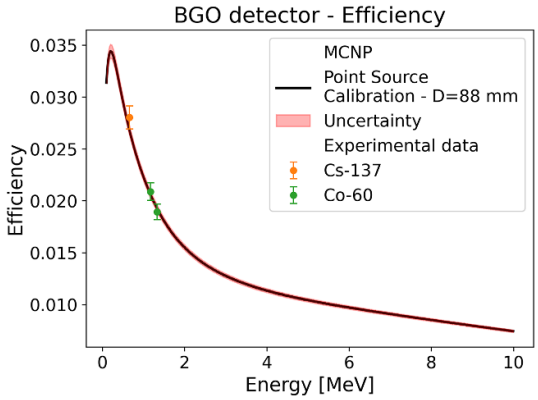

Figure 8. Detection efficiency of the BGO detector as a function of gamma ray energy. The black curve represents the corrected MCNP-simulated efficiency for a point source at a distance of 88 mm. The shaded red band shows the combined uncertainty taking into account statistical, geometric (±1 mm) and fit contributions. Experimental data from Cs-137 and Co-60 measurements are shown with 3% error bars (15 June 2024).

Table 3. Volumetric radiation source parameters and calculated BGO detection efficiency.

Parameter	Value
Diameter	15.24 cm
Length	228 cm
Volume	41.6 l
Energy	6.128 MeV
BGO efficiency	$9.27 \times 10^{-4} cps/(Bq/l)$

To evaluate the geometric uncertainty in the detection efficiency, calculations were performed by perturbing the source-to-detector distance by ± 1 mm, i.e. the estimated uncertainty in the distance. The calculated detection efficiencies vary between 1.1% and 1.6% (at low and high gamma energies). The statistical uncertainty is about 0.1%. The corrected BGO detector efficiency curve is shown in black in figure 8, the red area is represents the combined uncertainty due to the statistical uncertainties, the uncertainty in the source-to-detector distance and the uncertainties in the calibrated source activities. The experimental and calculated BGO detection efficiencies are presented in table 2.

4.2.1. Volumetric gamma source

In order to estimate the N-16 activity in the active water, the detection efficiency corresponding to the actual experimental setup was required. Calculations of the detection efficiency were performed for a volumetrically distributed N-16 gamma source in water in the cooling water pipe, with the lead collimator plates present.

The detection efficiency for the extended gamma source represents the ratio between the detected gamma rays per concentration of emitted gamma rays with the energy of interest for the simulated system. The parameters of the volumetric gamma source are listed in the table 3. The calculated total efficiency uncertainty of the BGO detector for the volumetric photon source at 6.13 MeV is about 3.5%, taking into account the geometrical uncertainty, the uncertainty of the scaling factor, the calibration uncertainty and the statistical uncertainty.

5. Water activation during JET DTE3 - C46 campaign

The JET—DTE3 WACT pulse database was filtered in order to consider only the discharges for which the experimental system was functioning normally. The BGO detector data were filtered based on neutron yield: High yield pulses ($n_{yeild} > 1.3 \times 10^{16}$) led to excessive water activation, resulting in increased count rates (BGO count rate > 100 *kcps*) that exceeded the DAQ bandwidth and caused data loss as shown in figure 9.

The neutron yield used in this work was obtained from the KN1 neutron diagnostic, which consists of three pairs of U-235/U-238 fission chamber detectors installed externally at designated octants around the JET tokamak. The KN1 system provides time-resolved measurements of total neutron emission and serves as the reference monitor for neutron yield during both DD and DT operation [14–16].

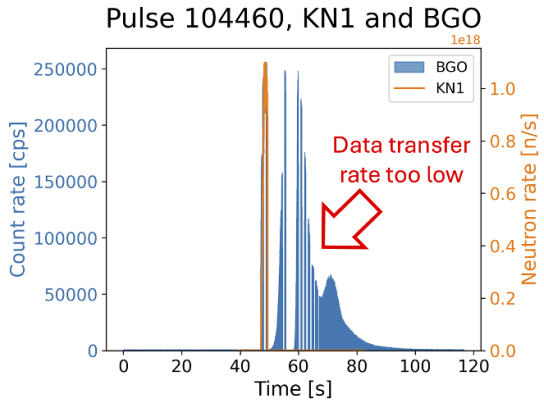

Figure 9. Time-resolved BGO detector γ signal and KN1 neutron signal for JET pulse 104 460. The high event rate exceeded the data transmission bandwidth, resulting in significant data loss and preventing a reliable determination of the total N-16 activity (26 September 2023).

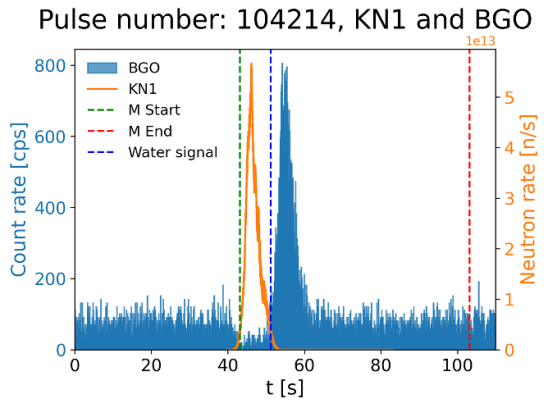

Figure 10. Time-resolved BGO detector γ signal and KN1 neutron signal for JET pulse 104 214, (8 September 2023). M start (green dashed line) and M end (red dashed line) indicate the start and end times of the gamma-ray spectrum acquisition window used for the analysis, with a fixed acquisition duration of 60 s. M start corresponds to the onset of neutron generation.

Figure 10 displays the temporal dependence of the recorded signals from the KN1 JET neutron monitor and the BGO detector, for a representative pulse. The total duration of the recording is 300 s. The JET plasma pulse starts at about $t \approx 40$ s (marked by the dashed green line), with a typical duration of up to 15 s. During this period, 14 MeV D–T neutrons are emitted and detected by the KN1 system (shown in orange). With an 9.5 s delay the gamma signal induced by activated cooling water starts marked by the dashed blue line. The signal from the BGO detector used to generate the pulse height spectra starts at the beginning of the plasma pulse (M start) for a total duration of 60 s and ends at the red dashed line (M End).

Figure 11 shows the energy spectra generated from the data for the previously defined time interval, where the characteristic peak of the N-16 decay in the range of 6 MeV due to water activation can be clearly recognized.

The area of the 6.13 MeV peak is determined for each selected pulse and corrected with the previously defined efficiency and correction factors presented in subsection 4.2. The N-16 radionuclide activity concentration is calculated as follows:

$$A_{\mathrm{N-16}} = \frac{N}{t_{\mathrm{m}} \cdot \epsilon_{\mathrm{vol}} \cdot I_{\gamma}}, \tag{1}$$

where N is the fitted peak area, t_{m} is the measurement time (live), ϵ_{vol} is the determined detection efficiency according to the extended source configuration and I_{γ} is the intensity of the 6.13 MeV N-16 gamma radiation [17]. The resulting data for all processed pulses are shown in figure 12. The data are divided into three categories based on detector performance and irradiation conditions. High pulse data refer to overexposed pulses, where high DT neutron yields caused excessive water activation and BGO count rates exceeded the data acquisition bandwidth, resulting in detector saturation and data

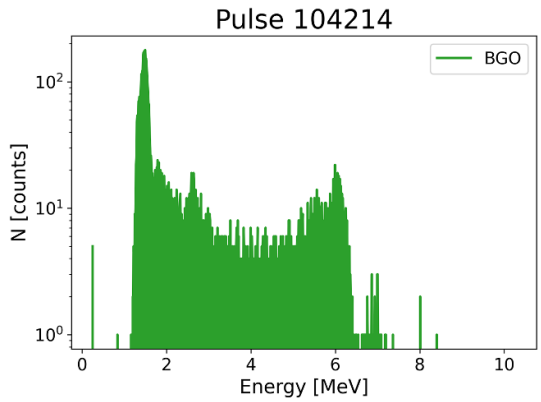

Figure 11. Energy spectra acquired with the BGO detector for JET pulse 104 223, (8 September 2023).

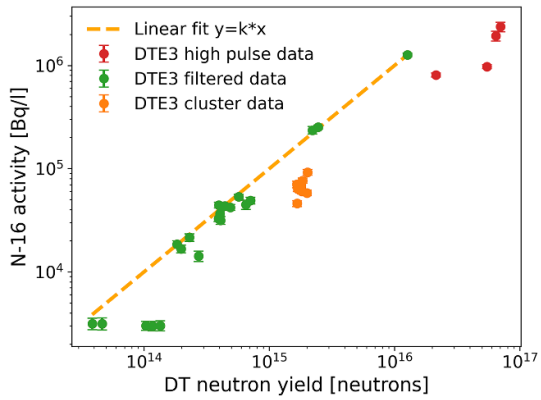

Figure 12. Correlation between the DT neutron yield and the N-16 activity measured with the BGO detector. Each data point represents a JET pulse. The orange dashed line indicates a linear fit to the data.

loss. Filtered data represent pulses for which the experimental system operated within its linear response range. Cluster data denote pulses for which the DT neutron yield alone would indicate operation within the linear regime; however, extended pulse durations led to detector overexposure.

The uncertainty of the measured N-16 activity includes contributions from the statistical uncertainty of the Monte Carlo transport, the geometric uncertainty due to the positioning of the experimental setup, the uncertainty of the scaling factor of the detector response, the uncertainty of the detector calibration and the uncertainty of the spectral processing. It is presented as a one standard deviation error bar.

The linear fit shown in figure 12(orange dashed line) was performed using the least squares method, assuming a linear model of the form $y = k \cdot x$, where y is the N-16 activity and x is the JET DT neutron yield. For the BGO detector, the fitted slope was determined to be $k = (9.96 \pm 0.007) \times 10^{-11}$ Bq/l·neutrons.

While the data with lower yields agree well with the linear fit, the points of the pulses with DT neutron yields higher than 1.3×10^{16} neutrons show a flattened response due to the saturation of the detector. Consequently, the N-16 signal no longer scales proportionally with the neutron yield, emphasizing the need for correction methods or alternative diagnostics in JET scenarios with high DT neutron yields.

The detector performance is not only influenced by the neutron yield, but also by the irradiation scenario, in particular the pulse duration. Longer pulses activate a larger volume of water, which increases the effective size of the source and leads to a higher average activity in the detector's field of view. This can lead to saturation of the detector even if the neutron yield remains below the nominal threshold. This explains why the orange data points deviate from the linear trend despite a moderate neutron yields, as the expanded activation volume creates a gamma field that exceeds the linear response range of the detector.

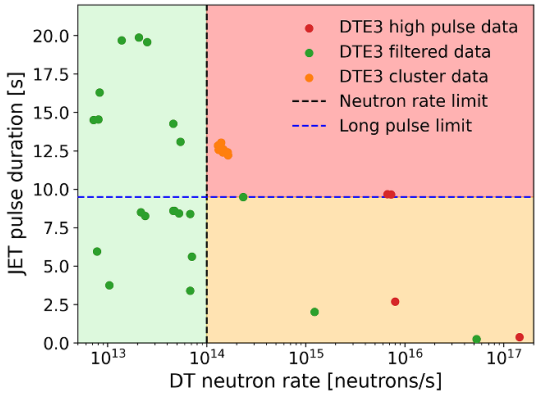

Figure 13. DT neutron rate as a function of JET pulse duration for the DTE3 campaign. Green symbols indicate pulses for which the BGO detector operated within its linear response range, orange symbols represent clustered data affected by extended pulse duration, and red symbols correspond to overexposed high pulses. The vertical dashed line denotes the neutron-rate limit, while the horizontal dashed line marks the long-pulse threshold (9.5 s), above which detector saturation occurs even at moderate neutron rates.

Figure 13 shows the distribution of pulse duration as a function of DT neutron rate for the analyzed DTE3 pulses, highlighting the combined effect of neutron rate and irradiation time on detector performance. Pulses with neutron rates below $1 \times 10^{14}\,\mathrm{n\,s^{-1}}$ (green region) consistently fall within the linear response range of the BGO detector. Pulses exceeding both the neutron rate limit and the pulse duration limit (red region) result in detector saturation. In contrast, pulses exceeding the neutron rate limit but with sufficiently short durations (orange region) can remain within the linear response range of the BGO detector.

The results presented in this paper show a linear correlation between the N-16 activity and the DT neutron yield. This confirms that the detector response remains linear within the investigated neutron yield interval, which extends up to 1.3×10^{16} neutrons. These results provide a solid basis for extrapolations to ITER operation scenarios, in which the neutron yield is expected to be significantly higher.

6. Conclusions

The water activation experiment conducted in the JET basement during the 2023 DD and DT campaigns represents the first successful measurement of fusion-relevant neutron-induced water activation in an operational tokamak environment.

The use of a lead-shielded BGO scintillation detector enabled the acquisition of gamma spectra for more than 1500 D–T plasma discharges. The study showed linear relationship between the DT neutron yield and the N-16 activity, confirming the reliability and linearity of the system over an operating range. Despite the problems with the NaI detector performance, the experimental setup provided a robust data set for fusion-relevant radiation analysis.

During DD operation, the water activation signal was significantly weaker and dominated by residual tritium; it was used primarily to validate the experimental setup. For this reason, DD results are not presented in detail in this paper and will be addressed in a dedicated future publication.

These results provide essential experimental data for the design and safety assessment of cooling systems in future D–T fusion reactors such as ITER, where water activation and radiation transport play a crucial role. As the only available measurements of water activation performed in a D–T fusion tokamak, they are of unique value for the validation of predictive models and the development of integrated diagnostic and simulation tools, including coupled fluid dynamics and neutronics codes, for future fusion devices.

The experiment validates the fundamental physical mechanisms of water activation by fusion neutrons, from neutron-induced production of N-16 to its transport and detection through high-energy gamma emission.

The experimental data generated in this study have been archived within the EUROfusion JET data infrastructure and are available to authorised users via the JET data access platform (https://users.jetdata.eu/) in accordance with EUROfusion data access and management policies.

Acknowledgments

The authors acknowledge the support of the Slovenian Research and Innovation Agency (Project Codes P2-0405 Fusion technologies; P2–0073 Reactor physics; PR-12326/PR-12842 Training of young researchers, NC-0022 Water activation in nuclear reactors). This work has been carried out within the framework of the EUROfusion Consortium, funded by the European Union via the Euratom Research and Training Programme (Grant Agreement No 101052200 — EUROfusion). Views and opinions expressed are however those of the author(s) only and do not necessarily reflect those of the European Union or the European Commission. Neither the European Union nor the European Commission can be held responsible for them.

Data availability statement

All data that support the findings of this study are included within the article (and any supplementary files).

Author contributions

Julijan Peric 0009-0003-9396-2574
Conceptualization (equal), Data curation (equal), Formal analysis (equal), Investigation (equal), Methodology (equal), Software (equal), Validation (equal), Visualization (equal), Writing – original draft (equal), Writing – review & editing (equal)

Domen Govekar
Data curation (equal), Formal analysis (equal), Writing – review & editing (equal)

Sebastjan Rupnik
Conceptualization (equal), Investigation (equal), Writing – review & editing (equal)

Luka Snoj
Funding acquisition (equal), Resources (equal), Supervision (equal), Writing – review & editing (equal)

Rosaria Villari
Conceptualization (equal), Formal analysis (equal), Funding acquisition (equal), Investigation (equal), Methodology (equal), Project administration (equal), Resources (equal), Supervision (equal), Validation (equal), Writing – review & editing (equal)

Nicola Fonnesu 0000-0002-2800-0040
Conceptualization (equal), Formal analysis (equal), Investigation (equal), Methodology (equal), Project administration (equal), Supervision (equal), Validation (equal), Writing – review & editing (equal)

Stefano Loreti
Data curation (equal), Formal analysis (equal), Investigation (equal), Methodology (equal), Resources (equal), Software (equal)

Perry Beaumont 0000-0002-4322-1677
Investigation (equal), Resources (equal)

Slawomir Mianowski
Resources (equal)

Callum Grove
Investigation (equal), Methodology (equal), Validation (equal), Writing – review & editing (equal)

Luke Jones
Resources (equal)

Tom Berry
Investigation (equal), Methodology (equal), Supervision (equal), Writing – review & editing (equal)

Chantal Shand 0000-0003-2259-8288
Funding acquisition (equal), Project administration (equal), Resources (equal), Supervision (equal), Writing – review & editing (equal)

Anthony Turner
Methodology (equal)

Haridev Chohan
Methodology (equal)

Paul Carman
Investigation (equal), Methodology (equal)

Robert Lobel
Investigation (equal), Methodology (equal), Resources (equal)

Marco De Pietri 0000-0002-2815-6889
Investigation (equal), Methodology (equal), Software (equal), Writing – review & editing (equal)

Eduardo Masia
Investigation (equal), Writing – review & editing (equal)

Aljaž Kolšek
Software (equal), Supervision (equal), Writing – review & editing (equal)

Raul Pampin
Software (equal), Writing – review & editing (equal)

Pierluigi Chiovaro 0000-0002-2851-9600
Validation (equal), Writing – review & editing (equal)

Vladimir Radulović
Conceptualization (equal), Formal analysis (equal), Funding acquisition (equal), Investigation (equal), Project administration (equal), Resources (equal), Supervision (equal), Writing – review & editing (equal)

References

[1] Radulović V, Rupnik S, Naish J, Bradnam S, Ghani Z, Popovichev S, Kiptily V, Batistoni P, Villari R and Snoj L 2021 *Fusion Eng. Des.* **169** 112410
[2] Žohar A and Snoj L 2019 *Prog. Nucl. Energy* **117** 103042
[3] Glasstone S and Lovberg R H 1960 *Controlled Thermonuclear Reactions* (D. Van Nostrand Company)
[4] Stacey W M 2010 *Fusion Plasma Physics* 2nd edn (Wiley)
[5] Romanelli F (JET EFDA Contributors) 2013 *Nucl. Fusion* **53** 104002
[6] Maggi C *et al* 2024 *Nucl. Fusion* **64** 112012
[7] Villari R *et al* 2025 *Fusion Eng. Des.* **217** 115133
[8] Wilson D, Ciric D, Cox S, Jones T, Kovari M, Li Puma A, Martin D, Milnes J, Shannon M and Surrey E 2007 *Fusion Eng. Des.* **82** 845–52
[9] Litaudon X *et al* 2024 *Nucl. Fusion* **64** 112006
[10] Waterhouse J, Wheatley M, Stephen A, Hogben C, Jones G, Goodyear A, Farmer T and McCullen P 2025 *Fusion Eng. Des.* **210** 114737
[11] Werner C J *et al* 2018 MCNP Version 6.2 Release Notes *Technical Report* LA-UR-18-20808 Los Alamos National Laboratory Los (available at: http://permalink.lanl.gov/object/tr?what=info:lanl-repo/lareport/LA-UR-18-20808)
[12] Nicolet J P and Erdi-Krausz G 2003 *Int. Atomic Energy Agency Technical Documents (IAEA-TECDOCs)* vol 1 p 173
[13] Kotnik D, Peric J, Govekar D, Snoj L and Lengar I 2025 *Nucl. Eng. Technol.* **57** 103233
[14] Batistoni P, Popovichev S, Conroy S, Lengar I, Čufar A, Abhangi M, Snoj L and Horton L JET Contributors 2017 *Rev. Sci. Instrum.* **88** 103505
[15] Batistoni P *et al* 2018 *Nucl. Fusion* **58** 106016
[16] Laszynska E, Batistoni P, Čufar A, Ghani Z, Jednorog S, Packer L and Popovichev S 2019 *Fusion Eng. Des.* **146** 1661–4
[17] Warburton E K, Alburger D E and Millener D J 1984 *Phys. Rev. C* **29** 2281–9